Behavior of eutectic Sn–Bi powder in Cu nanoparticle joints during the thermal treatment

S. Tajima, T. Satoh, T. Ishizaki & M. Usui

Journal of Materials Science: Materials in Electronics

ISSN 0957-4522

J Mater Sci: Mater Electron
DOI 10.1007/s10854-017-6602-6

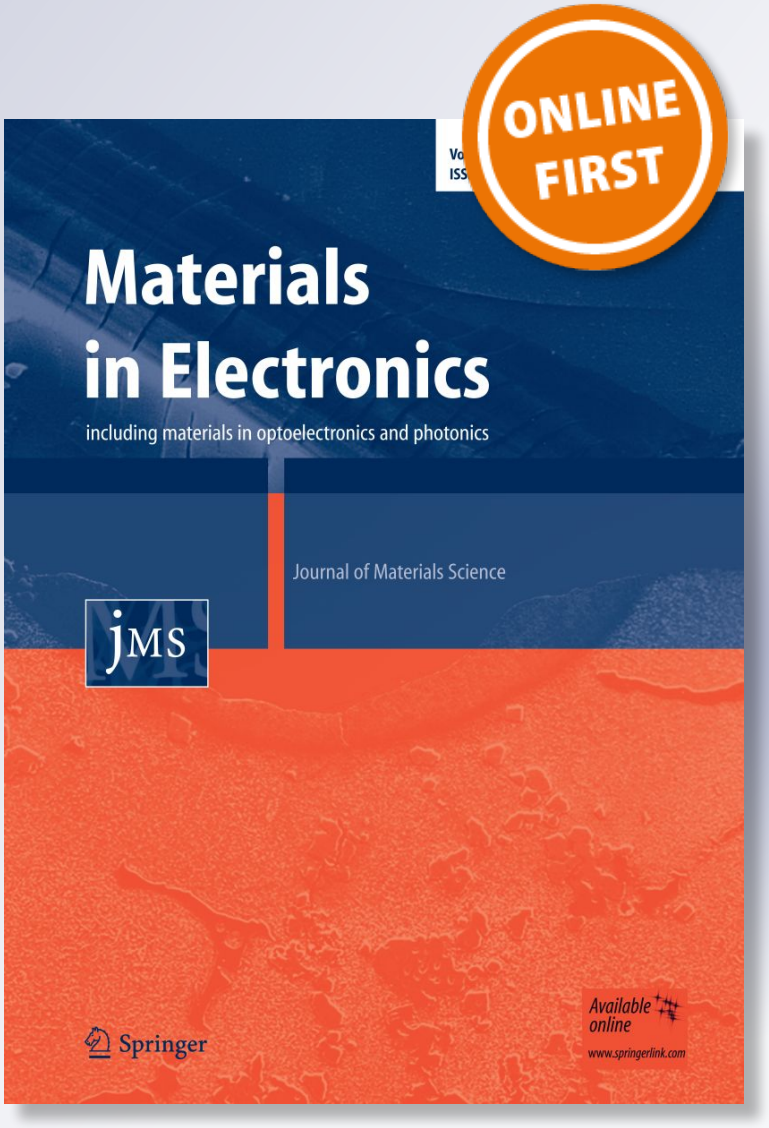

Springer

J Mater Sci: Mater Electron
DOI 10.1007/s10854-017-6602-6

Behavior of eutectic Sn–Bi powder in Cu nanoparticle joints during the thermal treatment

S. Tajima[1] · T. Satoh[1] · T. Ishizaki[1] · M. Usui[1]

Received: 10 January 2017 / Accepted: 14 February 2017

Abstract Ni-coated SiC chips and Cu substrates were joined by a paste of Cu nanoparticles and eutectic Sn–Bi powders as an alternative joint to conventional solders. The first thermal treatment of the joint was performed to melt eutectic Sn–Bi powders, while the second thermal treatment was conducted at 623 K for 5 min to eliminate the organic molecules around the Cu nanoparticles. The influence of the first thermal treatment conditions (423–473 K for 2–20 min) on the joint structure and strength was investigated. During the first thermal treatment conducted at 423 K for 20 min, or at 473 K for 2 min, Sn–Bi did not migrate to the nanoparticle area. During the second thermal treatment, Bi liquefied, migrated out of the powder, and segregated at the joint interfaces. This resulted in the formation of brittle interfaces and consequently a low bonding strength. In contrast, when the first thermal treatment was performed at 448 K for 20 min or 473 K for more than 5 min, liquefied Sn–Bi migrated out of the powder and segregated at the joint interfaces, where Bi subsequently reacted with the Ni layer at the interface to form Bi_xNi_y intermetallic compounds, which prevented the formation of a brittle interface and thus improved the bonding strength.

1 Introduction

SiC is a wide-band-gap semiconductor and a promising candidate to replace Si in power electronic devices, as operation of SiC-based power electronic devices at elevated temperatures can improve their power density [1, 2]. In order to operate such devices at high temperatures (above 523 K), the joint material connecting SiC chips and packaging materials must have high-temperature stability as well. Conventionally, tin-based solder alloys with melting points of ~500 K have been used as joint materials for Si-based power electronic devices. However, they cannot withstand the high junction temperature at which SiC-based devices operate [3, 4].

Metal nanoparticles have been considered to replace tin-based solder alloys due to their low sintering temperature (~473 K) and high-temperature stability (>523 K). Among various metals, Cu exhibits advantageous properties such as low cost, high resistivity against ion migration, high thermal conductivity (>125 W/mK), and resistance to thermal fatigue [5].

Since 2012, our group has been investigating the potential of Cu nanoparticles as a joint material for SiC-based power electronics devices. We first synthesized Cu nanoparticles encapsulated with fatty acids and amines and showed that those organic molecules could be dissociated at 623 K to sinter Cu nanoparticles [6]. We then evaluated the durability of such a Cu nanoparticle joint by connecting an Al_2O_3 heater chip and a Cu–Mo base plate in a device configuration designed to simulate the power cycle of SiC power electronic devices [7–9]. We found that further joint bonding strength improvement was necessary to meet the requirements of SiC power electronic device packaging.

In addition to several methods to improve the Cu nanoparticle joint bonding strength [10–16], optimization of the thermal treatment conditions has been shown to significantly influence the joint bonding properties [17]. Recently, we found that mixing a eutectic Sn–Bi atomized powder with Cu nanoparticles significantly improved the bonding strength and long-term reliability [18]. The Sn–Bi

✉ S. Tajima
stajima@mosk.tytlabs.co.jp

[1] Toyota Central R&D Labs., Inc., 41-1 Yokomichi, Nagakute, Aichi 480-1192, Japan

Published online: 26 February 2017

atomized powder is hereafter referred to as "powder" and the joint consisting of Cu nanoparticles and Sn–Bi powder as "CuSnBi joint." This newly developed CuSnBi joint was obtained by incorporating 14 at.% of eutectic Sn–Bi alloy powder to a Cu nanoparticle paste before performing the first and second thermal treatment in a H_2 atmosphere. The temperature of the first thermal treatment was set above the solidus line of the Sn–Bi alloy. Sn and Bi were therefore in a liquid state and could migrate to nanoparticle areas easily. The temperature of the second thermal treatmentwas above the dissociation temperature of the organic molecules around the Cu nanoparticles so that Cu nanoparticles sintered to form a strong joint.

We have been speculating that dispersion of liquid Sn and Bi into nanoparticle areas and wetting of the interface during the first thermal treatment stage, as well as the formation of an intermetallic compound (IMC) during the second thermal treatment stage, are crucial to enhancing the bonding strength [19–21]. However, the behavior of Sn and Bi during the first thermal treatment stage has not been studied in detail to confirm this hypothesis.

In this study, we investigated the contribution of the first thermal treatment to the enhancement of the bonding strength of the CuSnBi joint. In particular, we examined the effect of the first thermal treatment temperature and time. Optimal first thermal treatment conditions for the formation of a strong CuSnBi joint were proposed.

2 Methods and measurements

The synthesis of Cu nanoparticles encapsulated with fatty acids and amines has been explained in detail previously [6]. Briefly, 120 mmol of Cu carbonate ($CuCO_3{\cdot}Cu(OH)_2{\cdot}H_2O$: Wako Pure Chemical Industries, Japan) was reduced by 600 ml of ethylene glycol ($HO(CH_2)_2OH$: Wako Pure Chemical Industries, Japan), 180 mmol of decanoic acid ($C_9H_{19}COOH$; Wako Pure Chemical Industries, Japan), and 60 mmol of decyl amine ($C_{10}N_{21}NH_2$: Tokyo Chemical Industry, Japan) by stirring the mixture for 1 h at its boiling point in N_2 atmosphere. The Cu particles synthesized with a capping layer had an average diameter of 230 nm and are referred to as C10 Cu nanoparticles hereafter, where ten represents the carbon number of the fatty acid and amine. 0.24 g of an eutectic Sn–Bi (43 at.% Bi) powder (Kojundo Chemical Laboratory, Japan) was mixed with 0.56 g of C10 Cu nanoparticles. 60 µL of 1-decanol ($C_{10}H_{21}OH$: Wako Pure Chemical Industries, Japan) was then added to the mixture to make a paste, which was dried at 333 K for 2 h in vacuum prior to scanning electron microscopy/energy-dispersive X-ray spectroscopy (SEM/EDX) (SU3500, Hitachi High-Technologies, Japan) observations to determine the initial distribution of Sn and Bi in the C10 Cu nanoparticle paste.

4H-SiC(0001) and Cu substrates were pre-coated with sputtered Ti, Ni, and Ag films in order to improve their adhesion with nanoparticles [10, 11, 18]. Hereafter, "chip" refers to SiC/Ti (100 nm)/Ni (200 nm)/Ag (100 nm) and "substrate" to Cu/Ni (200 nm)/Ag (100 nm). Four 5 mm × 5 mm × 0.1 mm chips were placed on a 20 mm × 20 mm × 3 mm substrate as shown in Fig. 1a. The cross-section along A-A' in Fig. 1a showing the chip, joint, and substrate is depicted in Fig. 1b.

The sample shown in Fig. 1a was then mounted on a stainless steel sample holder, and a pressure of 0.5 MPa was applied with a spring plunger. Two thermal treatment stages were carried out in a H_2 atmosphere. Their temperature profile is shown in Fig. 2a. Three first thermal treatment temperatures (T_1 = 423, 448, or 473 K) and four first thermal treatment times (t_1 = 2, 5, 10, or 20 min) were tested in the first set of experiments. The distribution of Sn and Bi was then observed by SEM/EDX with an acceleration voltage of 15 kV and at a working distance of 10 mm. EDX mapping of Bi $M\alpha_1$, Sn $L\alpha_1$, Cu $L\alpha_1$, and Ni $K\alpha_1$ was also carried out.

In the second set of experiments, the samples underwent both thermal treatment stages following the temperature profile shown in Fig. 2b. After cooling, the samples were subjected to a shear test using a bond tester at a distance of 50 µm above the substrate and with a speed of 50 µm/s as is

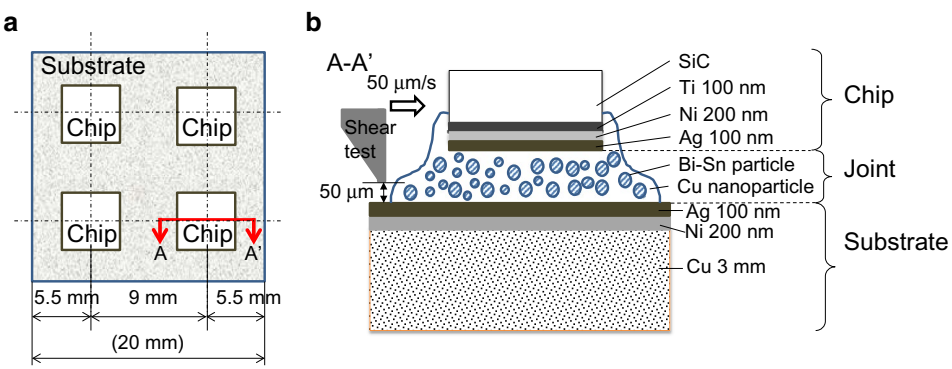

Fig. 1 Schematic of the joint sample used in this study. **a** Top view of the substrate and chips. **b** Cross-sectional view along A-A'

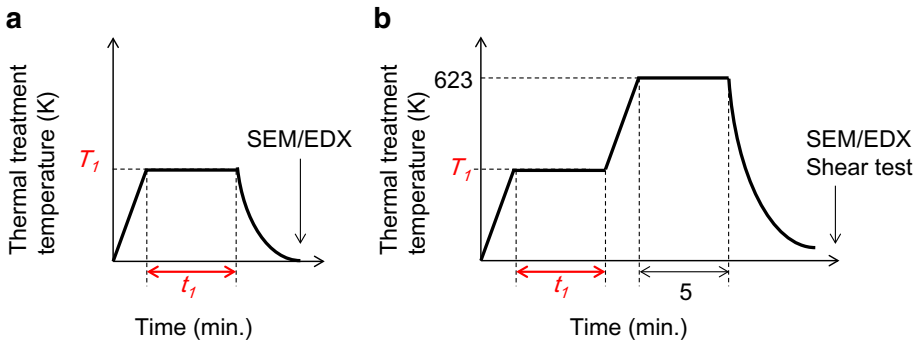

Fig. 2 **a** First thermal treatment temperature profile used for the first set of experiments. **b** First and second thermal treatment temperature profile used for the second set of experiments

shown in Fig. 1b. The bonding strength was calculated by dividing the shear force by the chip area (25 mm^2).

3 Results

3.1 Mixture of Sn–Bi powder and Cu nanoparticles priorc to the thermal treatment

Figure 3 shows the initial distribution of Sn–Bi powder and Cu nanoparticles in the paste before thermal treatment. Both Sn and Bi coexisted in the powder, and the powder was distributed evenly in the Cu nanoparticle paste. The diameter of the eutectic Sn–Bi powder was in the range 1–38 µm.

3.2 First thermal treatment (first set of experiments)

Figures 4 and 5 show cross-sectional SEM and Bi, Sn, Cu, and Ni EDX mapping images after first thermal treatment under different conditions.

The Ni sputtered film at the chip- and substrate-joint interfaces remained unchanged in terms of shape and chemical composition under all first thermal treatment conditions investigated.

Figure 4 shows images of samples subjected to a first thermal treatment for 20 min at different temperatures, T_1. When T_1 was 423 K (Fig. 4a), Sn and Bi remained in the powder, but their distribution within the powder changed with respect to that shown in Fig. 3. At this temperature, no obvious reaction between Cu and Sn was observed around the powder particles. For $T_1 \geq 448$ K, Sn and Bi were observed in Cu nanoparticle areas and at the joint interfaces, as shown in Fig. 4b, c. The majority of Bi atoms remained in the Sn–Bi alloy powder, while most of the Sn atoms were in the nanoparticle areas. As the T_1 value increased, the amount of Sn and Bi atoms present in the nanoparticle areas and at the interface increased. In contrast, the higher the T_1, the less Sn remained in the powder. The EDX images of Cu had two distinct contrasts. The gray areas correspond to areas where Sn atoms were also present, indicating the coexistence of Cu and Sn. Voids of irregular shapes were observed in the powder. As only Sn could react with Cu to form Cu_xSn_y, much more Sn migrated outside the powder than Bi, yielding a Bi-rich hypo-eutectic Sn–Bi powder. The voids thus correspond to a loss of Sn from the eutectic Sn–Bi.

In the next experiment, the time t_1 of the first thermal treatment was varied from 2 to 20 min while T_1 was 473 K. When t_1 was 2 min, the Sn and Bi atoms remained in the Sn–Bi alloy powder as shown in Fig. 5a. However, their distribution within the powder was different from the one observed in Fig. 3. Cu and Ni were observed in the joint and at the chip- and substrate-joint interfaces.

For $t_1 \geq 5$ min, Sn and Bi were observed in nanoparticle areas and at the joint interfaces (Fig. 5b, c, d. The

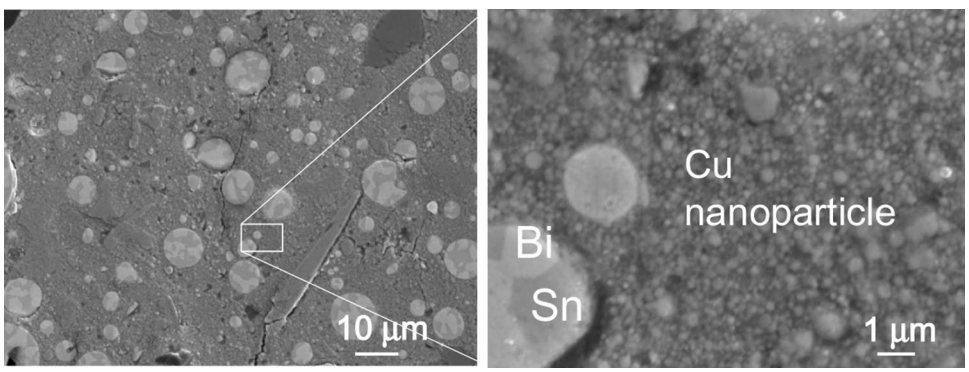

Fig. 3 Cross-sectional SEM images of eutectic Sn-Bi powder mixed in a Cu nanoparticle paste

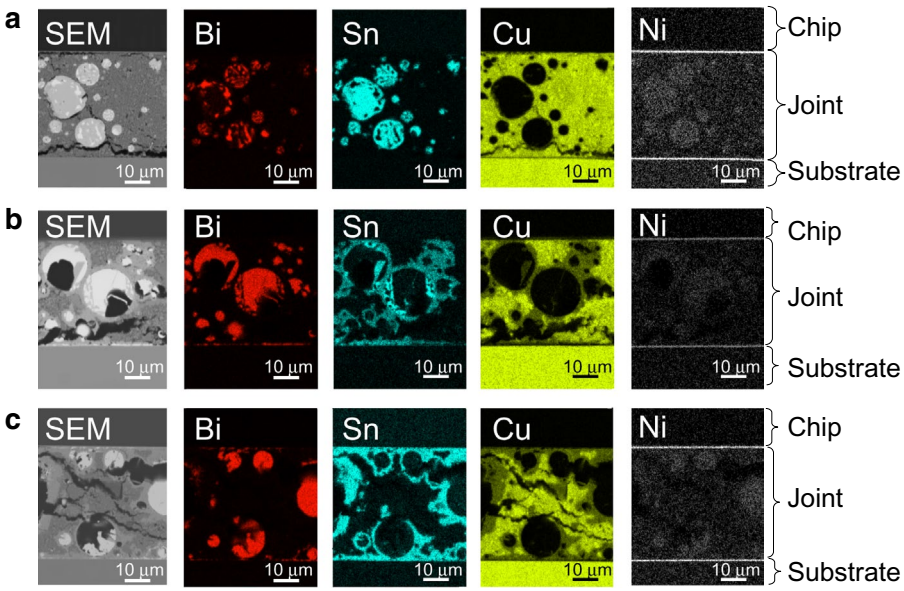

Fig. 4 Cross-sectional SEM and EDX mapping images after a 20 min-long first thermal treatment at a temperature T_1 of: **a** 423, **b** 448, and **c** 473 K

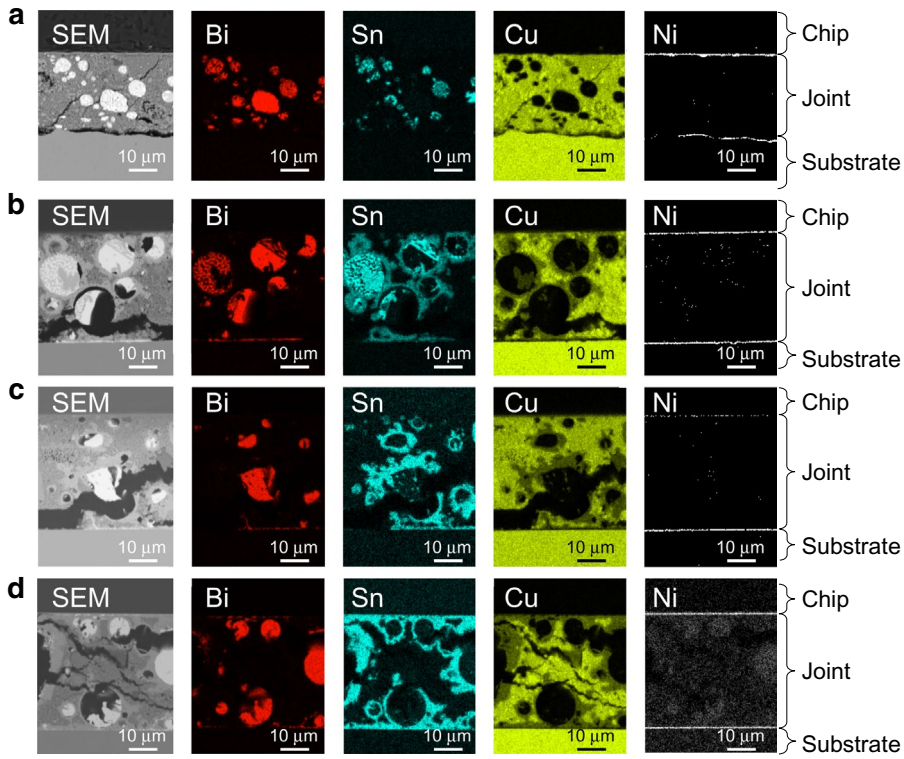

Fig. 5 Cross-sectional SEM and EDX mapping images after a first thermal treatment at a temperature T_1 of 473 K for a time t_1 of **a** 2, **b** 5, **c** 10, and **d** 20 min

Sn–Bi alloy powder mainly consisted of solid Bi and voids, while only a small quantity of Sn was still present. As in the previous experiment, the formation of voids was explained by the migration of Sn out of the powder. Areas containing Sn and Cu atoms were observed around the Sn–Bi alloy powder. The longer the t_1, the more Sn and Bi had migrated to the nanoparticle areas and the joint interfaces.

3.3 First and second thermal treatment (second set of experiments)

Multiple SEM and EDX mapping images were taken throughout the nanoparticle areas after completion of the two thermal treatment . Representative images are shown in Fig. 6. Figure 6a, b correspond to samples subjected to first thermal treatment for a time t_1 of

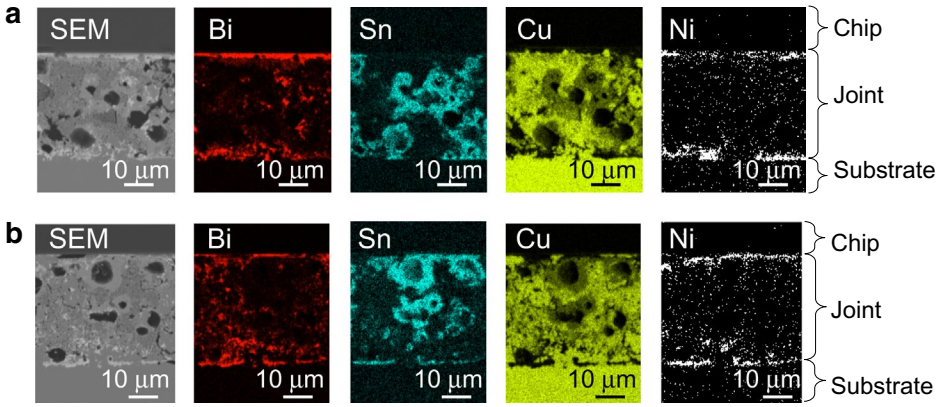

Fig. 6 Cross-sectional SEM/EDX images of samples having undergone a first thermal treatment for 20 min at **a** 423 K and **b** 473 K and a second thermal treatment at 623 K for 5 min

20 min at $T_1 = 423$ and 473 K, respectively. Sn and Bi were observed in the nanoparticle areas and at the joint interfaces, whereas there were only voids in place of the Sn–Bi powder particles. The majority of Cu nanoparticles sintered to form pure Cu, while the remaining ones consisted of Cu_xSn_y.

The differences between Fig. 6a, b demonstrate the influence of the first thermal treatment temperature, T_1, on the structure and chemical composition of the final product obtained after the second thermal treatment. For $T_1 = 423$ K, Bi tended to segregate at the joint interfaces, while Ni was found not only at the joint interfaces, but also in nanoparticle areas alongside Sn and Bi (Fig. 6a). For $T_1 = 473$ K, Bi was observed in nanoparticle areas, and formed a Bi–Ni alloy at the joint interfaces. More Ni was observed in nanoparticle areas in Fig. 6b with respect to Fig. 6a.

Figure 7 shows the results of the bonding strength of the CuSnBi joint measurements as a function of T_1 and t_1. For $T_1 = 423$ K and $t_1 = 20$ min, the bonding strength was ~14 MPa, which is the same value as that of a Cu nanoparticle joint without Sn–Bi powder. The bonding strength of the CuSnBi joint increased linearly with T_1 and t_1 as shown in Fig. 7a, b. The bonding strength of the CuSnBi joint was higher than that of a Cu nanoparticle joint (without Sn–Bi) for $T_1 \geq 448$ K (with $t_1 = 20$ min), or for $t_1 \geq 10$ min (with $T_1 = 473$ K). With $T_1 = 473$ K and $t_1 = 20$ min, the bonding strength of the CuSnBi joint was twice that of a Cu nanoparticle joint.

A fractional factorial design of experiment (DOE) was performed to decouple the effects of temperature and time on the bonding strength shown in Fig. 7. We found that both temperature and time were important factors that influence the bonding strength, but the effect of temperature was more significant than time.

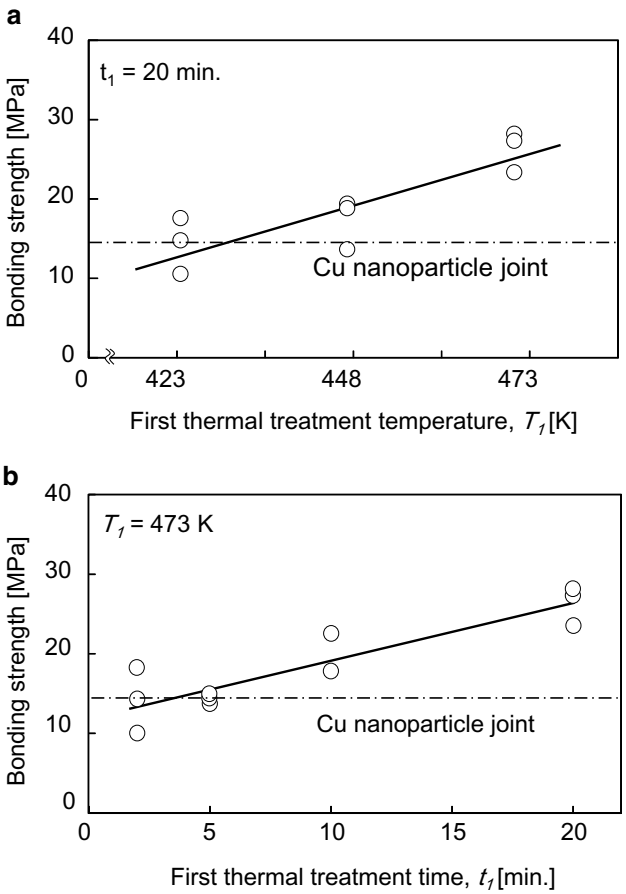

Fig. 7 **a** Bonding strength as a function of the first thermal treatment temperature, T_1, and **b** bonding strength as a function of the first thermal treatment time, t_1, of samples having undergone both thermal treatment

4 Discussion

The Sn–Bi alloy eutectic temperature is 412 K. Our results show that even with a first thermal treatment temperature slightly above the eutectic temperature ($T_1 = 423$ K), there was no migration of Bi and Sn atoms out of the powder.

A higher temperature reduces the liquid Sn–Bi viscosity, thus facilitating migration. The thermal treatment time was found to be another important parameter influencing the dispersion of Bi and Sn out of the powder.

Different migration behaviors of Sn and Bi in the joint were observed during the first thermal treatment (with $T_1 \geq 448$ K), and can be explained as follows. At the beginning of the first thermal treatment, the Sn–Bi alloy had just become liquid, and was still at the eutectic composition. After sufficient time (≥5 min), some Sn and Bi atoms migrated from the powder to the joint, but in different proportions. Sn and Cu could react to form an IMC (Cu_xSn_y) [22–24], while Bi could not form any IMC with Cu [25, 26]. Therefore, a larger fraction of Sn left the powder, yielding a hypo-eutectic Sn–Bi powder.

After completion of the first thermal treatment, the second thermal treatment was performed at 623 K. At this temperature, not only Sn-Bi alloy but also both Sn and Bi would become liquid since the melting point of Sn and Bi are 505 and 544 K, respectively. We observed that most of Sn and Bi migrated out of the powder, dispersed in the nanoparticle areas, and wetted the joint interfaces. Different first thermal treatment temperatures led to different final materials after completion of both thermal treatment. For instance, Bi tended to segregate after both thermal treatment when a low T_1 was selected, but no segregation was observed when a high T_1 was chosen. Furthermore, the amount of Ni dispersion in the Cu nanoparticles increased with increasing T_1. During the first thermal treatment stage at low T_1, Sn and Bi did not migrate in the nanoparticle areas, so that no IMC formed. As a result, there were still gaps between nanoparticles. These gaps allowed the dispersion of liquid Sn, Bi and Sn-Bi alloy between the nanoparticles during the second thermal treatment. Sn reacted with Cu, while Bi did not, and instead migrated further between the nanoparticles until it reached the joint interfaces, where it segregated. This Bi segregation led to a joint embrittlement, which in turn explains why the bonding strength of the CuSnBi joint was lower after a first thermal treatment at low temperature. During the first thermal treatment performed at high temperature, Cu_xSn_y formed in the joint. The Cu_xSn_y reduced the gaps between nanoparticles, hindering the dispersion of liquid Sn, Bi, and Sn–Bi alloy. Therefore, a majority of Bi atoms remained in nanoparticle areas, and thus did not segregate at the joint interfaces, leading to no embrittlement of the joint.

As for Ni, it was initially present as a film after the first thermal treatment. No reaction between Ni and Bi or Sn was observed during first thermal treatment since T_1 was always below the allotropic transformation temperature. During the second thermal treatment at 623 K, Sn and Bi became liquid and could react with Ni to form a liquid Bi–Ni alloy or Sn–Ni alloy. These liquid alloys could disperse in the nanoparticle areas to then form Bi_xNi_y [27–29] and Ni_xSn_y [30, 31] upon cooling. The higher the T_1, the more Sn and Bi atoms were present at the joint interfaces after completion of the first thermal treatment stage. Those Sn and Bi atoms could react with Ni at the joint interfaces at the beginning of the second thermal treatment. The formation of Cu_xSn_y, Bi_xNi_y, and Ni_xSn_y IMCs and the prevention of Bi segregation during the second thermal treatment stage are the main reasons for the bonding strength improvement upon addition of eutectic Sn-Bi alloy powder to the Cu nanoparticles.

5 Conclusions

In this paper, we investigate the mechanism behind the improvement in bonding strength and long-term reliability that was seen in earlier work, of Cu nanoparticles with the addition of mixing a eutectic Sn–Bi atomized powder. The behavior of Sn and Bi in the Cu nanoparticle joint during the first and second thermal treatment stages was studied to elucidate the cause of the joint bonding strength increase upon addition of eutectic Sn–Bi powder. The bonding strength of a CuSnBi joint increased linearly with an increase in temperature and time, and was higher than that of a Cu nanoparticle joint (without Sn–Bi). We found that Sn and Bi dispersion and wetting of the chip- and substrate-joint interfaces during the first thermal treatment was necessary to initiate the formation of IMCs during the second thermal treatment . Bi segregation or its absence after the completion of both thermal treatment was shown to result in joint embrittlement and strengthening, respectively. During the second thermal treatment, Bi–Ni alloy formation resulted in preventing Bi segregation and consequently improving the joint bonding. Thus, by optimizing the first thermal treatment conditions, the bonding strength of the CuSnBi joint could be doubled.

References

1. P.G. Neudeck, R.S. Okojie, L.Y. Chen, High-temperature electronics—a role for wide bandgap semiconductors? Proc. IEEE (2002). doi:10.1109/JPROC.2002.1021571
2. H.S. Chin, K.Y. Cheong, A.B. Ismail, A review on die attach materials for SiC-based high-temperature power devices, Metall. Mater. Trans. B (2010). doi:10.1007/s11663-010-9365-5
3. J.G. Bai, Z.Z. Zhang, J.N. Calata, G.Q. Lu, Low-temperature, sintered nanoscale silver as a novel semiconductor device-metallized substrate interconnect material. IEEE Trans. Compon. Packag. Technol (2006). doi:10.1109/TCAPT.2005.853167
4. J.G. Bai, G.Q. Lu, Thermomechanical, reliability of low-temperature sintered silver die attached SiC power device assembly. IEEE Trans. Device Mater. Rel (2006). doi:10.1109/TDMR.2006.882196

5. Y. Morisada, T. Nagaoka, M. Fukusumim, Y. Kashiwagi, M. Yamamoto, M. Nakamoto, A low-temperature bonding process using mixed Cu–Ag nanoparticles, J. Electron. Mater. (2010). doi:10.1007/s11664-010-1195-3
6. T. Ishizaki, R. Watanabe, A new one-pot method for the synthesis of Cu nanoparticles for low temperature bonding, J. Mater. Chem. (2012). doi:10.1039/C2JM34954J
7. T. Ishizaki, A. Kuno, A. Tane, M. Yanase, F. Osawa, Y. Yamada, Thermal characterizations of Cu nanoparticle joints for power semiconductor devices, Microelectron. Reliab. (2013). doi:10.1016/j.microrel.2013.07.042
8. T. Ishizaki, A. Kuno, A. Tane, M. Yanase, F. Osawa, T. Satoh, and Y. Yamada, Reliability of Cu nanoparticle joint for high temperature power electronics, Microelectron. Reliab. (2014). doi:10.1016/j.microrel.2014.07.113
9. T. Ishizaki, M. Usui, Y. Yamada, Thermal cycle reliability of Cu-nanoparticle joint, Microelec. Reliab. (2015). doi:10.1016/j.microrel.2015.07.039
10. T. Ishizaki, K. Akedo, T. Satoh, and R. Watanabe, Pressure-free bonding of metallic plates with Ni affinity layers using Cu nanoparticles, J. Electron. Mater. (2014). doi:10.1007/s11664-013-2953-9
11. T. Satoh, K. Akedo, T. Ishizaki, X-ray photoelectron spectroscopic study of the formation of Cu/Ni interface mediated by oxide phase, J. Alloys. Compd. (2014). doi:10.1016/j.jallcom.2013.08.042
12. R. Watanabe, T. Ishizaki, Enhancement of pressure-free bonding with Cu particles by the addition of Cu-Ni alloy nanoparticles. J. Mater. Chem. C (2014). doi:10.1039/C4TC00240G
13. R. Watanabe, T. Ishizaki, High-strength pressure-free bonding using nanoparticles. Part. Part. Syst. Charact (2014). doi:10.1002/ppsc.201300273
14. T. Satoh, T. Ishizaki, Enhanced pressure-free bonding using mixture of Cu and NiO nanoparticles, J. Alloy. Comp. (2015). doi:10.1016/j.jallcom.2014.12.224
15. T. Ishizaki, R. Watanabe, Pressureless bonding by use of Cu and Sn mixed nanoparticles, J. Electron. Mater. (2014). doi:10.1007/s11664-014-3368-y
16. M. Usui, H. Kimura, T. Satoh, T. Asada, S. Yamaguchi, M. Kato, Degradation of a sintered Cu nanoparticle layer studied by synchrotron radiation computed laminography. Microelectron. Reliab (2016). doi:10.1016/j.microrel.2016.06.011
17. T. Yamakawa, T. Takemoto, M. Shimoda, H. Nishikawa, K. Shiokawa, N. Terada, Influence of joining conditions on bonding strength of joints: efficacy of low-temperature bonding using Cu nanoparticle paste, J. Electron. Mater. (2013). doi:10.1007/s11664-013-2583-2
18. T. Satoh, T. Ishizaki, M. Usui, Nanoparticle/Solder hybrid joint for next-generation power semiconductor modules, submitted.
19. N.S. Bosco, F.W. Zok, Critical interlayer thickness for transient liquid phase bonding in the Cu–Sn system. Acta Mater. (2004). doi:10.1016/j.actamat.2004.02.043
20. F. Lang, H. Yamaguchi, H. Nakagawa, H. Sato, Thermally stable bonding of SiC devices with ceramic substrates: transient liquid phase thermal treatment using Cu/Sn powder. J. Electrochem. Soc. (2013). doi:10.1149/2.114308jes
21. O. Mokhtanri, H. Nishikawa, Transient liquid phase bonding of Sn–Bi solder with added Cu particles, J. Mater. Sci. (2016). doi:10.1007/s10854-016-4287-x
22. T. Ishihara, On the equilibrium diagram of the copper-tin system. J. Inst. Met **31**, 315 (1924)
23. H. Okamoto, Phase Diagrams for Binary Alloys. Desk Handbook, 2 edn. (ASM International, Materials Park, 2010), p. 321
24. N. Saunders, and A.P. Miodownik, The Cu-Sn (Copper-Tin) system, Bull. Alloy Phase Diagr. (1990). doi:10.1007/BF03029299
25. P. Cucka, C.S. Barrett, The Crystal Structure of Bi and of Solid Solutions of Pb, Sn, Sb and Te in Bi. Acta Crystallogr. (1962). doi:10.1107/S0365110X62002297
26. M. Ellner, K. Kolatschek, B. Predel, On the partial atomic volume and the partial molar enthalpy of aluminium in some phases with Cu and Cu_3Au structures, J. Less-Common Metals (1991). doi:10.1016/0022-5088(91)90062-9
27. H. Okamoto, *Phase Diagrams for Binary Alloys. Desk Handbook*, 2nd edn. (ASM International, Materials Park, 2010) p. 151
28. P. Nash, *Phase diagrams of binary nickel alloys*, (ASM International, Materials Park, 1991) p. 47
29. G.P. Vassilev, X.J. Liu, and K. Ishida, Experimental studies and thermodynamic optimization of the Ni-Bi system, J. Phase Equilibria Diffusion (2005). doi:10.1007/s11669-005-0134-0
30. H. Okamoto, *Phase Diagrams for Binary Alloys. Desk Handbook*, 2nd edn. (ASM International, Materials Park, 2010) p. 649
31. P. Nash, *Phase diagrams of binary nickel alloys*, (ASM International, Materials Park, 1991) p. 310